

Wavelet filters for programmable object investigation in digital holographic microscopy

M. MIHAILESCU*, A. M. PREDA, E. I. SCARLAT

Physics Department, University "Politehnica" of Bucharest, Romania

In this paper we present the application of the digital holographic microscopy in the investigation of a transparent object. In the experimental setup, based on the Mach-Zehnder interferometer with microscope objectives in both arms, we record on the CCD the hologram of a liquid crystal display, an electronically addressable device. The advantage of the digital processing of the recorded holograms is the fact that we can apply numerical filters (wavelet filter in our case), and study their effect in the contrast and the resolution of the fringe system, with the aim to eliminate the experimental aberrations. Based on the Fresnel transform, we simulate the propagation of the diffracted wave, after it passes through the hologram. Therefore we obtain information about the phase of the studied object when we address the same gray level or different gray levels on neighboring pixels. The simulation and experimental results are presented. Some parameters of the investigated object (birefringence, extraordinary refractive index, fill factor) were calculated.

(Received December 15, 2009; accepted January 20, 2010)

Keywords: Digital holographic microscopy, Wavelet filters, Fresnel transform, Phase, Mach-Zehnder, Liquid crystal display

1. Introduction

The digital holographic microscopy (DHM) is a suitable method for both the amplitude and phase investigation of the samples with details of sub-micrometric scale in the planes perpendicular to the optical axis. It is used in different domains like dynamic imaging in microbiology [1, 2], controlling and testing of the micro-opto-electro-mechanical systems [3]. Also, a spark-channel generated in air can be characterized [4]. The hologram obtained in the experimental setup is recorded on the charge coupled device camera array (CCD), transferred in computer like any image and transformed in numerical data. That permits its processing, filtering, physical phenomenon simulation with the aim to reconstruct the amplitude and the phase of the studied object.

The reconstruction process, which is based on the Fresnel-Kirchhoff integral, permits improvements in the reconstructed object image parameters such as the focus distance, the signal to noise ratio, the image size, the image resolution and also gives useful information for the calculation of the thickness and refractive index of the microscopic objects. One of the advantages of the DHM besides any microscopic techniques is the fact that from one single hologram recorded in the experimental setup, we can reconstruct different depths of the object [5], which is very important in time monitoring of the physical, biological, chemical and other processes. Besides this great depth of field, this method permits also a large field of view, both depending on the used objectives. From one single hologram, the studied object has few centimeters in planes perpendicular to the propagation axis [6].

We investigate a programmable liquid crystal display (PLCD). From fabrication data sheet we know its

thickness, constant over the entire surface, but its extraordinary refractive index varies in function of the gray levels applied through the corresponding voltages. Our results distinguish that the pixels with the same gray level introduce the phase shift which differs with less than 0.1° and we can calculate the birefringence; for the pixels with different gray levels we measure the differences in the optical path length (OPL) introduced between black and white levels. This technique allows us to see the boundary effect between two neighboring pixels and gives data for the calculation of the fill factor.

2. Digital holographic microscopy principles

Any holographic process involves two steps: the hologram recording and the object image reconstruction. In DHM the first step is experimental, and the second implies a numerical method based on the diffraction theory and on the filtering techniques, with the aim to visualize details from the object.

After the transparent sample is introduced in the object beam of the Mach-Zehnder interferometer (see Fig. 1), we record an image where both the reference and object wavefront interfere and the resulting intensity is:

$$I_H(x, y) = |R|^2 + |O|^2 + R^*O + RO^* \quad (1)$$

In the reconstruction process, the hologram is illuminated only by the reference wave:

$$I_{rec} = RI_H = R|R|^2 + R|O|^2 + |R|^2O + R^2O^* \quad (2)$$

The first two terms produce the zero order of diffraction, the third term produces a twin image and the

fourth produces the real image. In our case, the numerical reconstruction is based on the Fresnel diffraction pattern calculation at different distances z , starting with the real hologram.

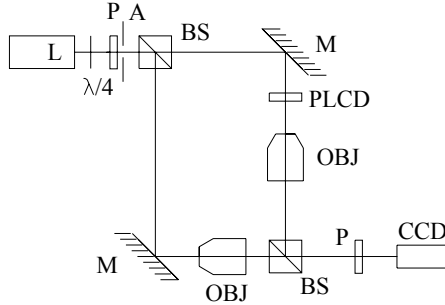


Fig. 1. A sketch of the Mach-Zehnder interferometer: L-laser (HeNe), A-aperture, BS-beam splitter, M-mirror, OBJ-microscope objective, S- sample (PLCD in this case), P-polarizers, CCD-video camera.

To obtain the image of the reconstructed object described by the complex field $O(x_1, y_1, z)$, in the plane of coordinates (x_1, y_1) at the distance z , we consider the hologram like a diffracting aperture with the transmission function $t(x_0, y_0)$, situated at $z = 0$, normally illuminated by a spherical laser wave. Using the 2-D convolution operator [7], we obtain:

$$O(x_1, y_1, z) = t(x_0, y_0, 0) \otimes h(x_0, y_0, x_1, y_1, z), \quad (3)$$

where $h(x_0, y_0, x_1, y_1, z) = \frac{\exp(ikr_{01})}{i\lambda r_{01}}$ is the impulse response, x_1, y_1 are the current coordinates in the output plane (the plane of the reconstructed object image), x_0, y_0 are the current coordinates in the input plane (hologram plane), $k = 2\pi/\lambda$, λ is the wavelength at which the hologram was recorded and r_{01} is the distance between any two points from the input plane to the output plane. We work in the Fresnel approximation in which we have $R_0 + R_1 < |z| < \frac{k(R_0 + R_1)^2}{8}$ where R_0 and R_1 are the radii of the apertures in the hologram plane and in the reconstructed object image plane. The impulse response from Eq. (3) becomes:

$$h(x_1, y_1, z) = \frac{\exp(ikz)}{i\lambda z} \exp\left\{\frac{ik}{2z} [x_1^2 + y_1^2]\right\} \quad (4)$$

In this case, the complex amplitude of the diffracted field from the Eq. (3) is given by:

$$O(x_1, y_1, z) = \frac{\exp(ikz)}{i\lambda z} \exp\left\{\frac{ik}{2z} [x_1^2 + y_1^2]\right\} \cdot \int_{-\infty}^{\infty} \int_{-\infty}^{\infty} O'(x_0, y_0, 0) \exp[-i2\pi(x_0 x_1 + y_0 y_1)] dx_0 dy_0 \quad (5)$$

where

$$O'(x_0, y_0, 0) = t(x_0, y_0, 0) \exp\left\{\frac{ik}{2z} [x_0^2 + y_0^2]\right\} \quad (6)$$

$O(x_1, y_1, z)$ is the 2-D Fourier Transform of the envelope $O'(x_0, y_0, 0)$ at spatial frequencies:

$$f_x = x_1 / \lambda z, f_y = y_1 / \lambda z \quad (7)$$

up to multiplicative amplitude and phase factors.

For the numerical calculation, we sampled these functions at Nyquist frequency and implemented the equations (5) and (6) in discrete form using 2-D matrices and the Fast Fourier Transform (FFT) routines in MATLAB. The dimensions of one pixel in the reconstructed object plane are linked with the dimensions of one pixel in the hologram plane by the relations [8]:

$$N\Delta x_1 \Delta x_0 = \lambda z \text{ and } M\Delta y_1 \Delta y_0 = \lambda z \quad (8)$$

where N, M are the total numbers of pixels in the x, y directions in both planes, $\Delta x_0, \Delta y_0$ are the dimensions of one pixel in the hologram plane and $\Delta x_1, \Delta y_1$ are the dimensions of one pixel in the plane of the reconstructed object. Therefore, in discrete form, the equations (5) and (6) become:

$$O(m\Delta x_1, n\Delta y_1, z) = \frac{\exp(ikz)}{i\lambda z} \cdot \exp\left\{\frac{ik}{2z} [(m\Delta x_1)^2 + (n\Delta y_1)^2]\right\} \cdot \sum_{m=1}^M \sum_{n=1}^N \{O'(m\Delta x_0, n\Delta y_0) \cdot \exp[-i2\pi(m^2\Delta x_0\Delta x_1 + n^2\Delta y_0\Delta y_1)]\} = Q_{FR}[t(m\Delta x_0, n\Delta y_0, 0)] \quad (9)$$

$$O'(m\Delta x_0, n\Delta y_0, 0) = t(m\Delta x_0, n\Delta y_0, 0) \cdot \exp\left\{\frac{ik}{2z} [(m\Delta x_0)^2 + (n\Delta y_0)^2]\right\}, \quad (10)$$

where $Q_{FR}[t(m\Delta x_0, n\Delta y_0, 0)]$ describes an operator named Fresnel transform which is applied to the transmission function of the hologram to obtain the whole field (amplitude and phase) in the reconstructed object plane, which can be written:

$$\begin{aligned}
O(m\Delta x_1, n\Delta y_1, z) &= \\
&= A(m\Delta x_1, n\Delta y_1, z) \cdot \exp[i\varphi_{real}(m\Delta x_1, n\Delta y_1, z)]
\end{aligned}
\tag{11}$$

Our object, proposed to investigate, is a programmable liquid crystal display (PLCD), which is an optoelectronic, computer addressed device, constructed like a sandwich, almost transparent, with a twist nematic liquid crystal layer in the middle. Different gray levels addressed from the computer to the neighboring pixels apply different voltages on them and the twist nematic liquid crystal molecules are rotated with different angles, which consequently introduce different extraordinary refractive index in the optical path length (OPL).

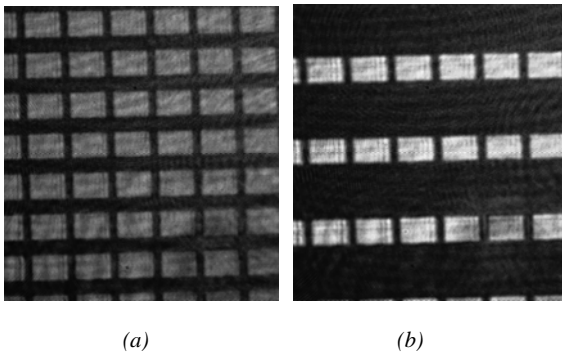


Fig. 2. The holograms of the programmable transparent object when we address (a) the same gray level on all pixels; (b) stripes of 1 pixel width with different gray Levels.

In the experimental setup, based on the Mach-Zehnder interferometer, with the investigated object in one arm, we record its digitized hologram on the CCD (see Fig. 2). Identical microscope objectives are used in the reference and object arms, to obtain waves with the same wavefront curvatures in the CCD plane. One single hologram (an intensity image) is sufficient to reconstruct the phase shift introduced by our transparent PLCD. We put two rotatable polarizers before and after our sample, because in the theory of the Jones matrix applied at PLCD, it is demonstrated that the parameters of the emergent wavefield from PLCD depends on the twist angle of the molecules θ and by the front director orientation [9].

In Fig. 2 (a) it is shown a hologram with the same gray levels on all PLCD pixels and in Fig. 2 (b) it is shown a hologram of the same region when we address some stripes on the PLCD (1 white pixel and 1 black pixel).

3. Holograms processing and object reconstruction

In order to start the reconstruction algorithm we need the holograms of the object in different states (see Fig. 2 (a) and 2 (b) and the reference hologram recorded without the object in the experimental setup (see Fig. 3 (a) and so

we calculate the phase delay introduced only by the PLCD subtracting the phase shift due to the interferometer [10].

If we apply a wavelet filter on the hologram recorded in the experimental setup, its Fourier spectrum is changed, which induces modification in the signal to noise ratio of the reconstructed object image. We used 5 discrete mother wavelets, with 1 to 5 resolution level, and we observed dramatically changing values in the approximation and the detail coefficients for 1–5 resolution level with each mother wavelet in the recorded holograms analysis.

In Fig. 3 (a) it is shown a part from the reference hologram acquired in the experimental setup and in Fig. 3 (b) it is shown the same reference hologram after we applied a wavelet decomposition based on mother haar of level 5. As one can see, the circular fringes from right bottom region (see Fig. 3a), due to experimental aberrations, are removed in the filtered image (see Fig. 3 (b)).

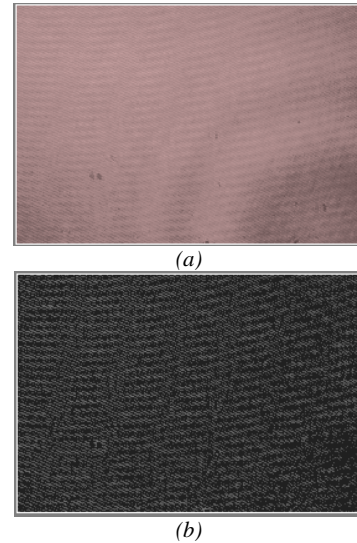


Fig. 3. Fringe pattern (a) with spherical aberrations and (b) corrected using wavelet filtering.

After the wavelet filtering, the Fourier spectrum of the hologram is calculated in MATLAB and the parasitic interferences, the zero-order and the twin image terms are eliminated (see Fig. 4). We follow this procedure for the reference hologram and also for the hologram acquired with the sample in the experimental setup.

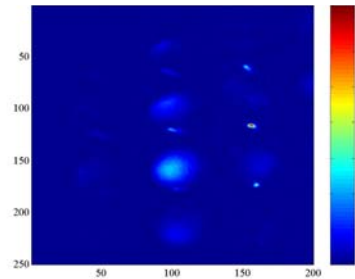


Fig. 4. The Fourier domain of the hologram with zero and -1 order eliminated.

An algorithm, based on the Fresnel approximation, implemented in its convolution mathematical form (described in the above section), it is used to reconstruct the images of the investigated object (see Fig. 5). The digital resolution in the z direction (the propagation direction) is of nanometer order and permits the reconstruction of different planes from the transparent object. To find the phase map of the object, several methods were used in the fitting process using dedicated software Koala (Zernike, polynomial).

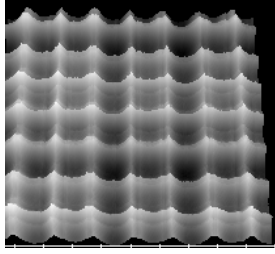


Fig. 5. The 3-D reconstructed image of the PLCD when a gray level map is addressed ($25\mu\text{m}$ between two consecutive divisions on the bottom scale).

4. Results and analysis

In MATLAB, we create a bi-dimensional (800×600 pixels) distribution of eight gray levels between 0 and 256 in the RGB mode, which are applied to the PLCD. Each of them introduced a different value of the potential V_{rms} which is electronically addressable on each cell of the PLCD. The applied potential is a linear function of the gray level for our 8-bit video digitizer and drive electronics (the producer gives $V_{rms} = 0,5\text{V}$ for white and $V_{rms} = 4,5\text{V}$ for black). The twist angle θ of the molecules in each cell depends on the applied voltage [11]:

$$\tan\left(\left(\frac{\pi}{2} - \theta\right)/2\right) = \exp\left[-\left(\frac{V_{rms} - V_t}{V_0}\right)\right] \quad (12)$$

where V_t is the threshold voltage below which no tilting of the molecules occurs and V_0 is the excess voltage.

The tilting of the liquid crystal molecules causes a reduction in the effective extraordinary refractive index $n_e(\theta)$:

$$\frac{1}{n_e^2(\theta)} = \frac{\cos^2(\theta)}{n_e^2} + \frac{\sin^2(\theta)}{n_o^2} \quad (13)$$

where n_e and n_o are the refractive indexes of the extraordinary and ordinary component without applied voltage, which determines the birefringence [12]

$\beta(V_{rms}) = \frac{\pi \cdot d \cdot (n_e(V_{rms}) - n_o)}{\lambda}$ where d is the thickness of the liquid crystal layer. In a twist nematic PLCD, the value of β can be changed applying voltage to the PLCD pixels. The real phase shift relatively introduced only by the liquid crystal layer, which is seen by the incident wave front of monochromatic, unit amplitude plane wave, is

$$\varphi_{real}(\theta) = \frac{2 \cdot \pi \cdot d \cdot (n_e(\theta) - n_o)}{\lambda} - \alpha_o \quad (14)$$

where α_o is the angle between the polarization direction of incident wave and optical axis of the PLCD, neglecting optical losses of the cell and phase shift introduced by the other layers (PLCD situated in the air).

From the complex function $O(m\Delta x_1, n\Delta y_1, z)$ (Ec. 9) we subtract the phase function given by $\varphi_{real}(m\Delta x_1, n\Delta y_1, z)$, which gives information about optical path length (OPL) introduced only by the sample itself. In our case, the thickness is constant from the fabrication considerations.

A profound study [13] of the behavior of the birefringence and the twist angle reveals that the birefringence has a step behavior in every cell, with a constant value in center, different for each applied voltage. This effect reduces the active area of each pixel.

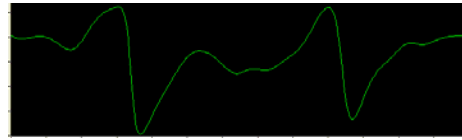


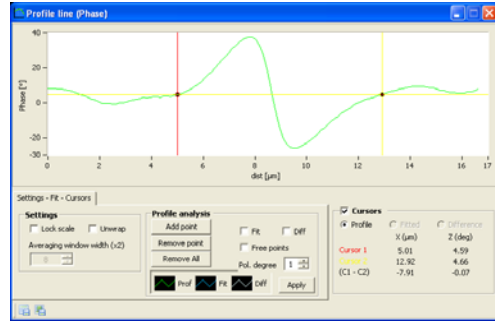
Fig. 6. Qualitative view of the perpendicular profile of the OPL at two consecutive pixels to distinguish the same shape of the boundary effect.

First of all, we recorded the hologram with inactive PLCD, with no voltage applied and we deduced the birefringence of the sample, $\beta_0 = 2.164$. When we addressed different potentials to some pixels, the extraordinary refractive index changes are perceived by the incident wave like different birefringence, phase and OPL.

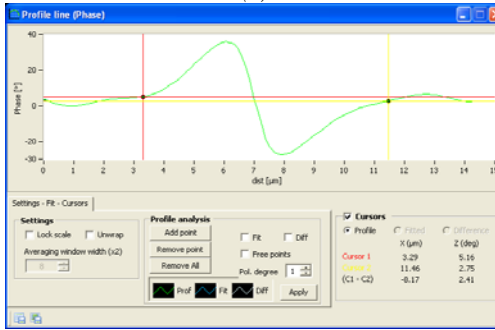
In Fig. 6 it is shown a qualitative view of the perpendicular profile of the OPL at two consecutive pixels to distinguish the same shape of the boundary effect.

Using cursors, we can measure the distances on which the boundary effect is visible in perpendicular profiles (see Fig. 7a, b) or in diagonal profile (see Fig. 7c), and also the phase shift, shown in Fig. 7a in perpendicular profile and in Fig. 7c in diagonal profile (The offset had been chosen with the zero point in middle). For two pixels with the same gray level addressed, the phase shift is less than 0.1° which is below standard deviation of the experimental measurements.

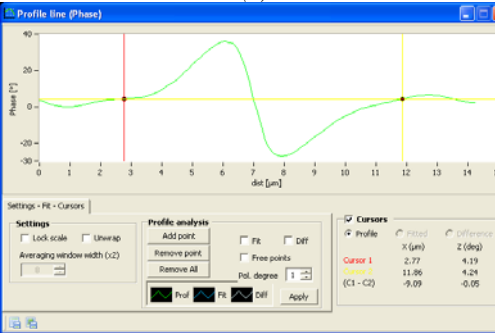
The boundary effect of $7.83\mu\text{m}$ and $8.27\mu\text{m}$ (mean values) represents 24.46% from the entire length between two pixels in the x direction and 25.84% in the y direction. The resulting fill factor 56.36% calculated after definition from [14] is in a good agreement with data sheet of the PLCD.



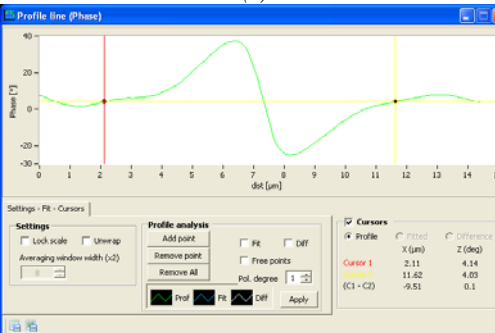
(a)



(b)



(c)



(d)

Fig. 7. Different profiles at the boundary between two pixels with the same gray level addressed (a) and (b) perpendicular profiles; c) and d) diagonal profiles.

Between pixels with different gray level addressed, using cursors we can measure the distances on which the boundary effect is visible and also the differences in the phase shift in perpendicular profiles (see Fig. 8a, b) or in diagonal profiles (see Fig. 8c, d).

From the measurements performed with cursors we recorded the maximum phase shift $\varphi_{real}(\theta_w) - \varphi_{real}(\theta_b) = 1,34\pi$ for angles of 20° and 70° between the PLCD optical axis and polarizer, respectively analyzer. At thickness $d = 1\mu\text{m}$ (from fabrication data) it corresponds to a $n_e(\theta_w) - n_e(\theta_b) = 0.442$, when we addressed to the PLCD 255 and 0 gray levels (corresponding with white and black levels), $\varphi_{real}(\theta_b)$ and $\varphi_{real}(\theta_w)$ is the phase shift introduced by the black and white level, $n_e(\theta_w)$ and $n_e(\theta_b)$ is the extraordinary refractive index in the same conditions.

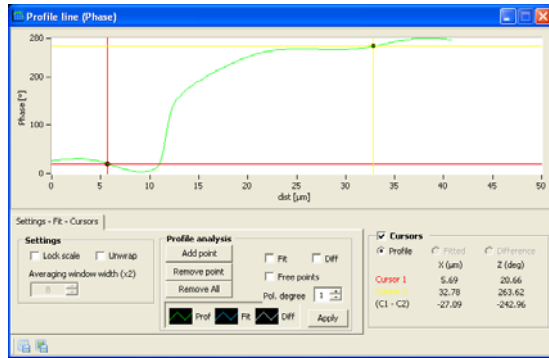
5. Discussion and conclusions

In this paper we present an application of the digital holographic microscopy in the programmable phase object investigation. Processed holograms using wavelet filters allow the removal of the unwanted residuals. The best level of the mother function has been found after sorting out 5 discrete mother wavelets, with 1 to 5 resolution levels. After that, in the reconstruction process the standard method has been followed.

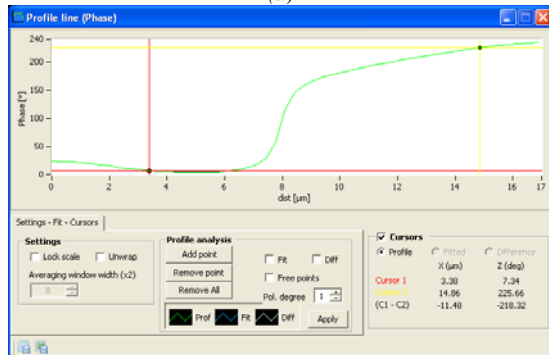
A PLCD screen is composed from many finite elements (pixels). The size of the electrodes of the picture elements is finite, and that causes boundary effects in the phase distribution. In order to examine the edge effects, we addressed the same gray levels on the neighboring pixels of the PLCD.

The calibration for the phase shift was done without any voltage applied on the PLCD. In this case, we deduced the birefringence of the sample, $\beta_0 = 2.164$. The profiles taken in different points between two neighboring pixels with the same gray level addressed reveal that the difference in the phase shift is negligible (less than 0.1°). In the image of the reconstructed object, abrupt variations at the boundary between two neighboring pixels are distinguished in perpendicular and diagonal profile, and the resulting fill factor is 56.36%.

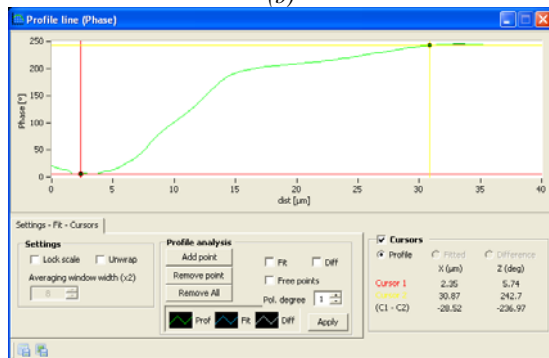
The difference between the birefringence when the white and the black level is addressed to the PLCD, reveals a phase difference of about $1,34\pi$ and a difference in the extraordinary refractive index of 0.442 when the PLCD was sandwiched between two rotatable polarizers.



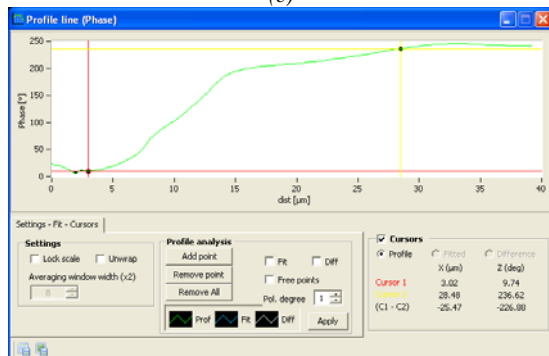
(a)



(b)



(c)



(d)

Fig. 8. Different profiles at the boundary between two pixels with different gray level addressed (a) and (b) perpendicular profiles; (c) and (d) diagonal profiles.

DHM is an alternative method which permits more than visualizing micrometric objects with nanometric details in z direction. It gives the basic information useful to determine some physical properties of the sample, such as birefringence, refractive index, thickness, deformation.

Acknowledgements

The experiments described in this paper were carried out using equipments acquired by Contract 4/CP/I/11.09.2007 PNCDI II "Capacities" and the research has been (partially) supported by the ANCS-UEFISCSU grant ID 1556 / 2009.

References

- [1] B. Rappaz, A. Barbul, Y. Emery, R Korenstein, C. Depeursinge, P. J. Magistretti, P. Marquet, *Cytometry* **73A**, 895 (2008).
- [2] J. Schnekenburgera, I. Bredebuscha, W. Domschkea, B. Kemperb, P. Langehanenberg, G. von Ballyb, *Medical Laser Application* **22**, 165 (2007).
- [3] Chuan Qin, Jianlin Zhao, Jianglei Di, Le Wang, Yiting Yu, Weizheng Yuan, *Appl. Opt.* **48**, 919 (2009)
- [4] M. Mihailescu, L. Preda, A.M. Preda, E. I. Scarlat, *J. Opt. Adv. Mat.* **10**, 623 (2008).
- [5] V. Mico, Z. Zalevsky, C. Ferreira, J. Garcia, *Opt. Express* **16**, 19260 (2008).
- [6] Jianglei Di, Jianlin Zhao, Hongzhen Jiang, Peng Zhang, Qi Fan, and Weiwei Sun, *Appl. Opt.* **47**, 5654 (2008).
- [7] J. W. Goodman, Mc Graw-Hill Book Company, chapter 2, 1968.
- [8] J. Garcia, D. Mas, R. G. Dorsch, *Appl. Opt.* **35**(35), 7013 (1996).
- [9] A. Hermerschmidt, S. Quiram, F. Kallmeyer, H. J. Eichler, *Proc. of SPIE* **6587**, 65871B (2007).
- [10] M. Paturzo, P. Memmolo A. Tulino, A. Finizio, P. Ferraro, *Opt. Expr.* **17**(11), 8709 (2009).
- [11] C. Soutar, K. Lu, *Opt. Eng.* **33**(8), 2704 (1994).
- [12] A. Yariv, P. Yeh, *Optical Waves in Crystals*, John Wiley & Sons, 1984.
- [13] A. Marquez, J. Campos, M. J. Yzuel, I. Moreno, J. A. Davis, C. Iemmi, A. Moreno, A. Robert, *Opt. Eng.* **39**(12), 3301 (2000).
- [14] P. J. Rodrigo, V. R. Daria, J. Glückstad, *Opt. Expr.* **13**, 1384 (2005).

*Corresponding author: mona_m@physics.pub.ro